Thin–Walled Structures 197 (2024) 111519

Contents lists available at ScienceDirect

Thin-Walled Structures

journal homepage: www.elsevier.com/locate/tws

Full length article

Thin-walled tapered conformable low-pressure tanks: Concept and principles

Joren Malfroy [a,*], Ben Van Bavel [a], Johan Steelant [a,b], Dirk Vandepitte [a]

[a] KU Leuven, Department of Mechanical Engineering, Celestijnenlaan 300, B-3001, Leuven, Belgium
[b] Flight Vehicles and Aerothermodynamics Engineering Section, Noordwijk, The Netherlands

ARTICLE INFO

Keywords:
Pressure tank
Conformable
Multi-bubble
Multi-lobe
Multi-cell
Tapered

ABSTRACT

In pressure tank design, structural efficiency or the ratio of pressurized volume to structural mass is fundamental and implies a specific shape, such as a cylindrical or spherical layout. However, this axi-symmetric layout may be not conform to the enveloping shape. Previous investigations developed a conformable tank concept with a multi-bubble axi-symmetric layout, called a multi-lobe, multi-cell or multi-bubble tank, but structural design and analysis are limited to intersecting cylindrical, spherical or toroidal shells. The objective of this research is to increase the volumetric efficiency of multi-bubble tanks even further through the introduction of a conical shell. An integral analytical formulation of tank topology and explicit expression of equilibrium are provided in order to design a structurally efficient tapered multi-bubble tank under low differential pressure. The result is expressed in a geometric rule that is applicable for tapered multi-bubble tanks of any eligible shape.

1. Introduction

Classical pressure tanks have an axi-symmetric layout, which is the most effective structural concept to cope with differential pressure without bending stress in the tank wall. Cylindrical pressure tanks with domed ends are common in many engineering applications to store or transport liquid or gas under pressure. If a significant amount of liquid or gas is to be stored, however, the accommodation of single cylindrical pressure tanks requires a large volume and is often inconsistent with the general layout of the host cavity.

The concept of a conformable pressurized structure or multi-bubble tank provides a solution. Multi-bubble tanks consist of intersecting shells with web reinforcements. Compared with classical pressure tanks, multi-bubble tanks take full advantage of the available space and offer the lowest structural weight when volumetric efficiency and conformability are important. In a context of variable topology bubbles can adapt to the convex or concave contour of the available space. Unlike unpressurized fuel tanks, which do not have strict restrictions on shape and size, a multi-bubble tank is subject to additional specifications on its geometrical design. Not only should each bubble of the tank have a three-dimensional convexity, the fact that it is pressurized implies a specific shape. Fig. 1 illustrates the two-dimensional concept of a multi-bubble structure with intersecting circular shells. The vertical members, usually referred to as webs, are required to transfer the circumferential forces as a result of the differential pressure. The connection between two circular shells and a web is called the Y-junction. Translation of the multi-bubble cross section shown in Fig. 1 gives a cylindrical multi-bubble structure or multi-cylinder, revolution around the horizontal transverse axis gives a spherical multi-bubble structure or multi-sphere and revolution around the vertical transverse axis gives a toroidal multi-bubble structure or multi-torus. Fig. 2 shows an example of an open multi-bubble structure with a cylindrical layout. This paper studies conformable pressure tanks under uniform internal pressure. In a similar context, analytical formulations for the stress analysis of egg-shaped sludge digestors [1,2] and spherical multi-bubble tanks [3] under internal hydrostatic pressure are described by Zingoni. A pressure tank in the form of a barrelled shape and loaded with a uniform external pressure is presented by Jasoin [4].

In 1972, Ardema published a first article on the integration of pressurized conformable structures in hypersonic aircraft in search of optimum structural mass and volumetric efficiency of the tank within an elliptic envelope [5]. This framework was used in 2020 by Van Bavel and subsequently in 2022 by Malfroy to optimize the volumetric efficiency of the central multi-bubble tank in a hypersonic vehicle concept [6,7]. The application of intercontinental hypersonic transportation is already on the drawing tables for a long time, and conformable pressurized tanks are particularly of interest to store the cryogenic propellants in a liquid state on board of the LAPCAT MR2.4 vehicle [8–10], the STRATOFLY MR3 vehicle [11–13] and the X-33 vehicle [14]. Multi-bubble tanks are also interesting for application as a pressure cabin [15–17] or cargo transport fuselage [18] in blended wing body aircraft. The LAPCAT and STRATOFLY programmes are

* Corresponding author.
E-mail address: joren.malfroy@kuleuven.be (J. Malfroy).

https://doi.org/10.1016/j.tws.2023.111519
Received 13 June 2023; Received in revised form 17 October 2023; Accepted 18 December 2023
Available online 21 December 2023

Nomenclature

Latin letters

G	Implicit function
N	Normal force per unit length
p	Internal pressure
Q	Transverse force per unit length
r	Radius
t	Membrane thickness
v	Distance between two axes of revolution
x	Horizontal transverse direction
y	Vertical transverse direction
z	Longitudinal direction

Greek letters

α, β	Taper angle
γ	Angle between two axes of revolution
δ	Angle between the web and the z-axis in the plane containing the axes of revolution
θ	Circumferential direction
σ	Stress

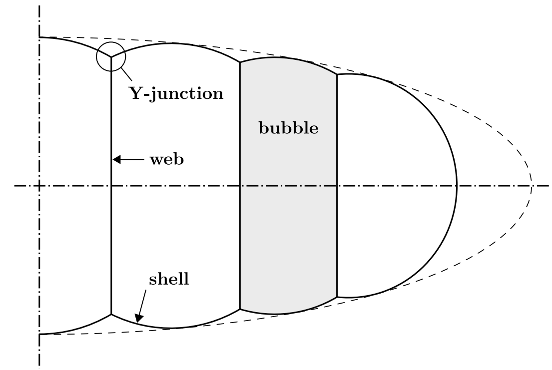

Fig. 1. Half the cross section of a seven-bubble tank (solid line) in an elliptic envelope (dashed line).

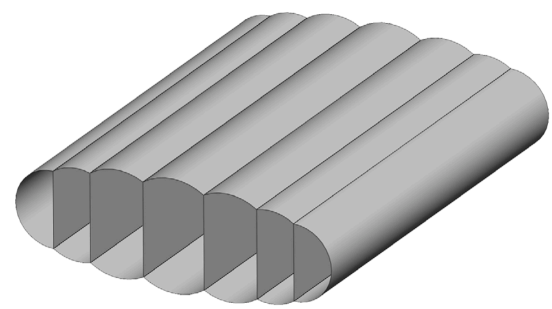

Fig. 2. Example of a cylindrical multi-bubble structure.

European research development projects on hypersonic flight vehicles with strong restrictions on the geometric space to accommodate conformable liquid hydrogen pressure tanks [19]. The main advantages of using hydrogen fuel are its high gravimetric energy density and the absence of carbon-based pollution in the exhaust after combustion with air. Liquid hydrogen needs to be stored in pressure tanks at cryogenic temperatures and low pressure to maintain the liquid state of the fuel.

In 2012, Geuskens improved the understanding in the design and analysis of conformable pressurized structures with a cylindrical, spherical and toroidal layout [20–22]. Scientific research is limited to the analysis of these three multi-bubble configurations and the volume optimization of conformable tanks is therefore limited to two dimensions. The addition of a taper degree of freedom for each bubble provides much more freedom for accommodating the tank in a surrounding structure with arbitrary shape. Multi-bubble tanks with bubbles tapered along their longitudinal axis have the potential to maximize the volumetric efficiency. When designing a tapered multi-bubble tank, bending stress in the tank wall must be minimized which would otherwise reduce the structural efficiency considerably. One of the most important conclusions in the work of Geuskens is that membrane forces in multi-bubble tanks can be visually assessed by taking into consideration the complete set of distinctive geometry descriptors. For this reason, a fully analytical formulation using a complete set of geometry descriptors for a thin-walled tapered multi-bubble structure is preferred over a numerical simulation using the finite element method. The analytical model should also facilitate optimization strategies to fit the tapered multi-bubble tank to a prescribed volume in further research.

Tapered multi-bubble tanks with full spatial freedom have not been realized yet, mainly due to an insufficient understanding of conformable pressurized structures. This paper investigates the structural feasibility of the thin-walled tapered multi-bubble structure. Section 2 defines the geometry of a tapered multi-bubble structure using conical shells in a three-dimensional Cartesian coordinate system and elaborates on the shape of the web. The analytical model of the primitive shapes of the geometry leads to an analytical formulation of stress resultants and equilibrium in Section 3. The analytical formulation is limited to force equilibrium considerations at the Y-junction. Localized shell bending due to incompatibilities in the membrane deformations of adjacent shell edges, e.g. at the junction of a dished head and a cylindrical shell [23], is not considered. Section 4 discusses the relation that results between the planarity of the web and the structural efficiency of the tank and Section 5 verifies the accuracy and applicability of the analytical solution by comparison with a static structural finite element analysis of a tapered multi-bubble tank with multi-spherical heads. Sensitivity of the planarity of the web to the structural efficiency of the tank is shown in Section 6.

2. Geometry descriptors

This section is an introduction to the geometry of a tapered multi-bubble tank and defines a complete set of geometry descriptors.

2.1. Cylindrical multi-bubble tank

A cylindrical multi-bubble tank is an assembly of multiple intersecting cylindrical shells with parallel axes of revolution. If in addition all axes of revolution lie in the same plane, then this plane is a plane of symmetry of the multi-bubble tank. Fig. 3 shows a cross section of a cylindrical multi-bubble tank and a set of five geometry descriptors in two intersecting cylinders (Table 1): two radii r, two angles θ that define the boundary of the cylindrical shells and a separation distance v between the two axes of revolution. In each pair of cylinders two geometrical relations hold in the two-dimensional space xy:

$$r_1 \cos\theta_1 + r_2 \cos\theta_2 = v \tag{1}$$

$$r_1 \sin\theta_1 - r_2 \sin\theta_2 = 0 \tag{2}$$

Consequently, each pair of cylinders of a cylindrical multi-bubble tank is completely defined by a set of three independent geometry descriptors $\Psi = \{r_1, r_2, v\}$. The total set of geometry descriptors $\Psi = \{r_1 \dots r_N, v_1 \dots v_{N-1}\}$ with $N \geq 2$ the number of bubbles in the multi-bubble tank gives an unambiguous and complete description of the cross section of an arbitrary cylindrical multi-bubble tank.

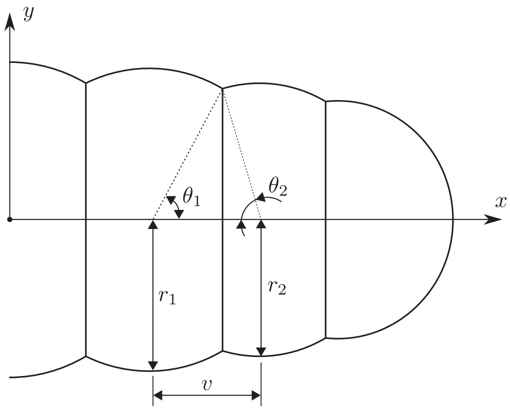

Fig. 3. Geometry descriptors in two intersecting cylinders of a cylindrical multi-bubble tank.

Table 1
Definition of the geometry descriptors in two intersecting cylinders of a cylindrical multi-bubble tank.

Symbol	Definition
θ_i	Angle between the plane containing the axes of revolution and the radius of the ith cylinder intersecting the circle in the Y-junction
r_i	Radius of the ith cylinder
v	Distance between the axes of revolution

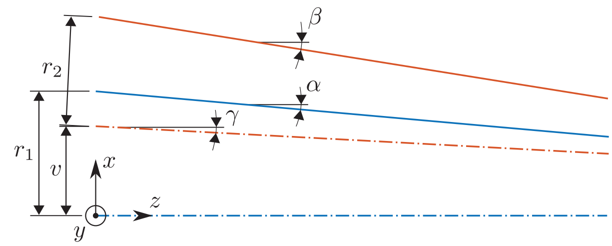

Fig. 4. Independent geometry descriptors in two intersecting cones of a tapered multi-bubble tank. This illustration shows the first cone (blue), second cone (orange) and axes of revolution (dash-dotted line). (For interpretation of the references to colour in this figure legend, the reader is referred to the web version of this article.)

Table 2
Definition of the geometry descriptors in two intersecting cones of a tapered multi-bubble tank.

Symbol	Definition
α	Half apex angle of the ith cone
β	Sum of the half apex angle of the $(i+1)$th cone and the angle γ
γ	Angle between the axes of revolution
δ	Angle of deflection of the web
θ_i	Angle between the plane containing the axes of revolution and the radius of the ith cone intersecting the circle in the Y-junction
r_i	Largest radius of the ith cone
v	Largest distance between the axes of revolution

2.2. Tapered multi-bubble tank

Design of cylindrical multi-bubble tanks is inherently limited to the two-dimensional space. A tapered multi-bubble tank is now added with design degree of freedom in the third direction. The tapered layout that is the most effective to cope with differential pressure is found in the primitive axi-symmetric shape of a conical shell. A tapered multi-bubble tank is therefore an assembly of multiple intersecting conical shells with parallel or intersecting axes of revolution. If in addition all axes of revolution lie in the same plane, then this plane is a plane of symmetry of the multi-bubble tank. Fig. 4 defines two intersecting cones as two individual shells of revolution. A three-dimensional coordinate system xyz is defined at the centre of the largest circle with radius r_1 of a first cone with the z-axis centred along the axis of revolution of that cone. The axis of revolution of a second cone with largest radius r_2 starts at an offset v along the x-axis and intersects the axis of revolution of the first cone at an angle γ. The first and second cones have apex angles 2α and $2(\beta-\gamma)$, respectively, with $\beta \geq \gamma$. The angles $\alpha, \beta \in [0, \pi/2)$ and $\gamma \in (-\pi/2, \pi/2)$ are defined clockwise and represent additional degrees of freedom in the design of the tank in the third dimension. Consequently, each pair of cones of a tapered multi-bubble structure or multi-cone is fully represented by a set of six independent geometry descriptors $\Psi = \{\alpha, \beta, \gamma, r_1, r_2, v\}$ (Table 2).

Fig. 5 shows a three-dimensional example of a tapered multi-bubble structure. In contrast to the intersection of two cylindrical shells with parallel axes of revolution, the intersection of two conical shells with coplanar axes of revolution is a space curve. The web is the curved surface that contains the space curve and is perpendicular to the plane containing the axes of revolution. An analytical model of the intersection is found starting with the description of the first cone and second cone in Cartesian coordinates. The implicit equation of the first cone $G_{c,1}(x, y, z)$ for which the largest radius r_1 is linearly decreasing at an angle α along the longitudinal z-axis is:

$$G_{c,1}(x, y, z) = x^2 + y^2 - (r_1 - z\tan\alpha)^2 = 0 \tag{3}$$

The implicit form of the second cone $G_{c,2}(x, y, z)$ is similar to Eq. (3) but replacing r_1 by r_2 and α by $(\beta-\gamma)$. After a clockwise rotation around the y-axis at an angle γ and subsequently a translation along the x-axis by a distance v in accordance with Fig. 4 the equation reads:

$$\begin{aligned} G_{c,2}(x, y, z) &= [(x-v)\cos\gamma + z\sin\gamma]^2 + y^2 \\ &\quad - \left[r_2 + ((x-v)\sin\gamma - z\cos\gamma)\tan(\beta-\gamma)\right]^2 = 0 \end{aligned} \tag{4}$$

Eqs. (3) and (4) provide an analytical description of the three-dimensional intersection in the xyz coordinate system. The subtraction of both equations eliminates the dependency on y because of the coplanar character of the axes of revolution which results in a bivariate quadratic function:

$$\begin{aligned} G_w(x, z) &= G_{c,2}(x, y, z) - G_{c,1}(x, y, z) \\ &= Ax^2 + Bxz + Cz^2 + Dx + Ez + F = 0 \end{aligned} \tag{5}$$

Derivation of the coefficients A-F is elaborated in Appendix:

$$A = -\frac{\sin^2\gamma}{\cos^2(\beta-\gamma)} \qquad B = \frac{\sin 2\gamma}{\cos^2(\beta-\gamma)}$$
$$C = -A - \tan^2(\beta-\gamma) + \tan^2\alpha$$
$$D = -2v(1+A) - 2r_2\sin\gamma\tan(\beta-\gamma)$$
$$E = -vB + 2r_2\cos\gamma\tan(\beta-\gamma) - 2r_1\tan\alpha$$
$$F = -vD - v^2(1+A) - r_2^2 + r_1^2$$

Eq. (5) shows the projection $x(z)$ of the space curve given by $G_{c,1}(x(z), y, z) = 0$ onto the plane containing the axes of revolution such that $G_w(x(z), z) = 0$. Implicit differentiation of $G_w(x(z), z) = 0$ with respect to z gives:

$$\frac{\partial G_w}{\partial z} + \frac{\partial G_w}{\partial x}\frac{\mathrm{d}x}{\mathrm{d}z} = 0 \tag{6}$$

The web's angle of deflection δ is the angle between the web and the z-axis in the plane containing the axes of revolution, is defined to be positive if $x(z)$ is decreasing and is obtained using Eq. (6):

$$\tan\delta(z) = -\frac{\mathrm{d}x}{\mathrm{d}z} = \frac{Bx(z) + 2Cz + E}{2Ax(z) + Bz + D} \tag{7}$$

Fig. 6 shows a geometrical interpretation of the angle $\delta(z)$. Eq. (7) shows that the angle $\delta(z)$ depends on z, which implies that the web

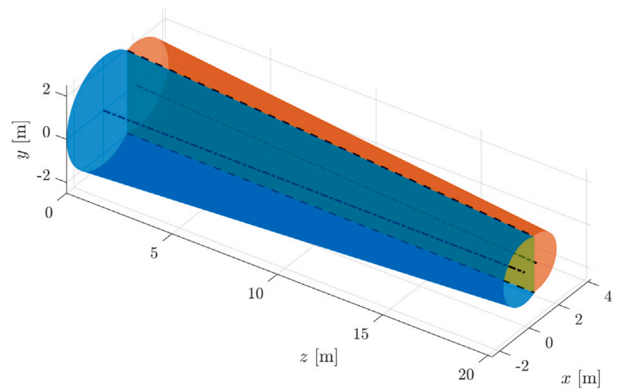

Fig. 5. Example of a tapered two-bubble structure with $\{r_1, r_2, v\} = \{2.5, 2.0, 2.2\}$ m and $\{\alpha, \beta, \gamma\} = \{3, 6, 4\}$ degrees. This illustration shows the first cone (blue), second cone (orange), web (green), intersection curve (dashed line) and axes of revolution (dash-dotted line). (For interpretation of the references to colour in this figure legend, the reader is referred to the web version of this article.)

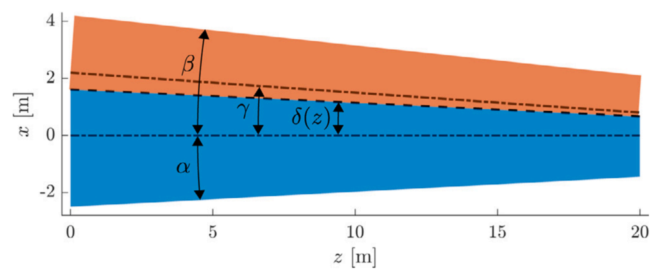

Fig. 6. Top view of the example in Fig. 5 and a geometrical interpretation of the angles α, β, γ and $\delta(z)$.

is in general nonplanar. The discriminant $B^2 - 4AC$ shows that $x(z)$ is a hyperbola for every set $\{\alpha, \beta, \gamma \mid \gamma \neq 0°\}$ and a parabola if $\gamma = 0°$. The concavity of the hyperbolic or parabolic function on the other hand depends on the total set of independent geometry descriptors $\{\alpha, \beta, \gamma, r_1, r_2, v\}$. Hence, at least one solution exists for γ for every set $\{\alpha, \beta, r_1, r_2, v\}$ such that the intersection of two conical shells is a plane curve resulting in a planar web. This condition is met if the second order derivative of x with respect to z is equal to zero. Implicit differentiation of Eq. (6) with respect to z gives:

$$\frac{\partial^2 G_w}{\partial z^2} + 2\frac{\partial^2 G_w}{\partial x \partial z}\frac{\mathrm{d}x}{\mathrm{d}z} + \frac{\partial^2 G_w}{\partial x^2}\left(\frac{\mathrm{d}x}{\mathrm{d}z}\right)^2 + \frac{\partial G_w}{\partial x}\frac{\mathrm{d}^2 x}{\mathrm{d}z^2} = 0 \tag{8}$$

While the factor $\frac{\partial G_w}{\partial x}$ in the fourth term is always nonzero by definition, the second order derivative of x with respect to z is equal to zero in Eq. (8) if and only if the following condition is met:

$$\frac{\partial^2 G_w}{\partial z^2} + 2\frac{\partial^2 G_w}{\partial x \partial z}\frac{\mathrm{d}x}{\mathrm{d}z} + \frac{\partial^2 G_w}{\partial x^2}\left(\frac{\mathrm{d}x}{\mathrm{d}z}\right)^2 = 0 \tag{9}$$

with

$$\frac{\partial^2 G_w}{\partial z^2} = 2C, \quad \frac{\partial^2 G_w}{\partial x \partial z} = B, \quad \frac{\partial^2 G_w}{\partial x^2} = 2A$$

Eq. (9) leads to

$$-A - \tan^2(\beta - \gamma) + \tan^2\alpha - B\tan\delta + A\tan^2\delta = 0 \tag{10}$$

Trigonometric identities (see Appendix) simplify Eq. (10) to the elegant expression:

$$\cos(\gamma - \delta)\cos\alpha = \cos\delta\cos(\beta - \gamma) \tag{11}$$

In conclusion, the angle δ does not change along the longitudinal z-axis, the intersection is a plane curve and the web is a plane surface if and only if Eq. (11) is satisfied. Parameters $\{r_1, r_2, v\}$ are included in Eq. (11) via Eq. (7).

3. Equilibrium of forces

Any (conformable) thin-walled pressurized tank is structurally efficient, i.e. the ratio of pressurized volume to structural mass is maximized, if the orientation of the members align with the orientation of resulting forces which are transferred by each of the members. Shells of revolution have the property that under axi-symmetric loading perpendicular to the shell, membrane stress is dominant. Each bubble of the conformable tank must therefore be a shell of revolution and any deviation from the shell of revolution (e.g. an elliptic cylinder) gives rise to bending moments in the wall which reduce the structural efficiency considerably [21].

3.1. Cylindrical multi-bubble tank

Fig. 7 shows the stress resultants between three structural members at a Y-junction in a cylindrical multi-bubble tank. For a cylinder with radius r subject to an internal pressure p [Pa], the hoop force N_θ [N/m], i.e. the normal force along the circumferential direction θ per unit length of section, is given by

$$N_\theta = pr$$

According to the definitions of Flügge, all forces are defined per unit length and division of the normal force by membrane thickness gives the normal stress in the shell element [24]. The normal force N_y and the transverse force Q_x in the web where two cylindrical shells meet are found from the expression of force equilibrium along the y- and x-axes, respectively:

$$\begin{aligned} N_y &= N_{\theta,2}\cos\theta_2 + N_{\theta,1}\cos\theta_1 \\ &= p\left(r_2\cos\theta_2 + r_1\cos\theta_1\right) \end{aligned} \tag{12}$$

$$\begin{aligned} Q_x &= N_{\theta,2}\sin\theta_2 - N_{\theta,1}\sin\theta_1 \\ &= p\left(r_2\sin\theta_2 - r_1\sin\theta_1\right) \end{aligned} \tag{13}$$

The transverse force Q_x should vanish to minimize bending moments in the structure. Eq. (13) shows that Q_x is equal to zero if the following condition is met:

$$r_1\sin\theta_1 = r_2\sin\theta_2 \tag{14}$$

A closer look to the geometry descriptors in Fig. 3 shows that Eq. (14) is identical to Eq. (2) which is a geometrical constraint that should always hold. As a result, any cylindrical multi-bubble tank is structurally efficient as Q_x is always zero. Further reformulation of Eq. (12) using Eq. (1) gives a geometrical interpretation of the normal force in the web of a cylindrical multi-bubble tank:

$$N_y = pv$$

3.2. Tapered multi-bubble tank

The two-dimensional methodology to describe the stress system in a cylindrical multi-bubble tank is now extended to a methodology in three dimensions for the tapered multi-bubble tank defined in Fig. 4. In a tapered multi-bubble configuration, however, the analytical description of equilibrium of forces at a Y-junction is more involved as the radii of the shells change along their axial direction, the axes of revolution are intersecting lines and the web is in general a curved surface due to the introduction of the angles α, β and γ. Because of the curvature of the web, a curvilinear coordinate system with orthogonal axes, one of which is perpendicular to the surface of the web, is required to define the transverse direction of the web. Fig. 8 shows the orthogonal curvilinear coordinate system with y' and z' the coordinate axes tangent to the surface of the web and x' the transverse coordinate axis perpendicular to the surface of the web. The directions y and y' are parallel.

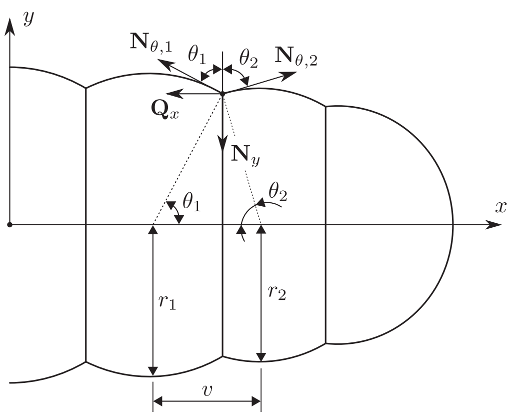

Fig. 7. Stress resultants at a Y-junction in a cylindrical multi-bubble tank.

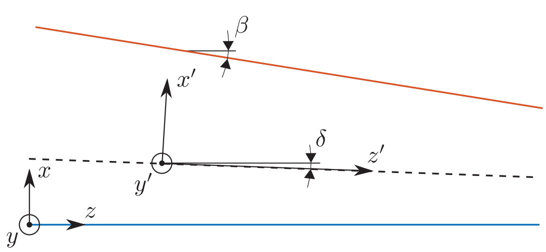

Fig. 8. Simplification of Fig. 6 to show the orthogonal curvilinear coordinate system $x'y'z'$ at the intersection (dashed line) of two conical shells with x' the direction perpendicular to the surface of the web.

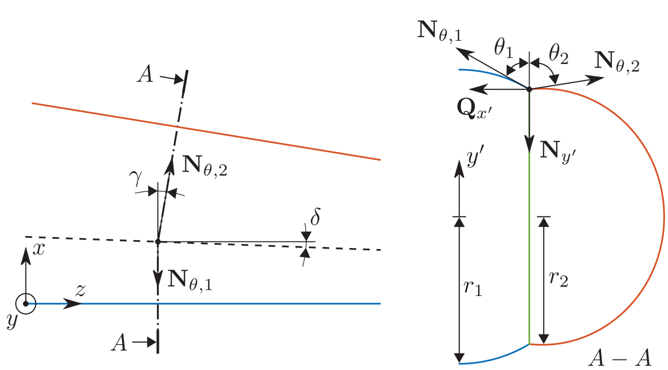

Fig. 9. Stress resultants at a Y-junction in an arbitrary section $A-A$ of a tapered multi-bubble tank.

Fig. 9 shows the stress resultants at a Y-junction in a tapered multi-bubble tank. Similar to the cylindrical multi-bubble tank, the tapered multi-bubble tank is structurally efficient if transverse forces vanish everywhere. For a conical shell subject to an internal pressure p, the hoop force per unit length is expressed as

$$N_\theta = \frac{pr}{\cos\alpha}$$

where r is the distance of one of its points from the axis of revolution and 2α is the apex angle of the cone. The hoop force N_θ is a normal force along the circumferential direction which is perpendicular to the axis of revolution, as shown at the left in Fig. 9. The normal force $N_{y'}$ and the transverse force $Q_{x'}$ in an arbitrary section of the web where two conical shells meet are calculated by expressing force equilibrium along the y'- and x'-axes, respectively:

$$\begin{aligned} N_{y'} &= N_{\theta,2}\cos\theta_2 + N_{\theta,1}\cos\theta_1 \\ &= p\left(\frac{r_2\cos\theta_2}{\cos(\beta-\gamma)} + \frac{r_1\cos\theta_1}{\cos\alpha}\right) \end{aligned} \tag{15}$$

$$\begin{aligned} Q_{x'} &= N_{\theta,2}\sin\theta_2\cos(\gamma-\delta) - N_{\theta,1}\sin\theta_1\cos\delta \\ &= p\left(r_2\sin\theta_2\frac{\cos(\gamma-\delta)}{\cos(\beta-\gamma)} - r_1\sin\theta_1\frac{\cos\delta}{\cos\alpha}\right) \end{aligned} \tag{16}$$

Eq. (15) describes the normal force $N_{y'}$ in the web. It simplifies to Eq. (12) if both shells are cylindrical shells, i.e. $\alpha = 0°$ and $\beta = \gamma$. Eq. (16) shows that the transverse force $Q_{x'}$ vanishes if the following two conditions are met:

$$r_1\sin\theta_1 = r_2\sin\theta_2 \tag{17}$$

$$\cos(\gamma-\delta)\cos\alpha = \cos\delta\cos(\beta-\gamma) \tag{18}$$

Section 4 gives a thorough discussion of the two conditions expressed in Eqs. (17) and (18).

4. Discussion

Eq. (17) is identical to Eq. (14) and is met for every cone that is merged with another cone as long as the axes of revolution are coplanar, which is by definition always the case. Eq. (18) is identical to Eq. (11) and is therefore always guaranteed if the intersection of two conical shells is a plane curve. This observation leads to the Equivalence which states that a thin-walled tapered multi-bubble tank with N bubbles under differential pressure is structurally efficient if all $(N-1)$ webs are plane surfaces.

Equivalence. *A thin-walled tapered multi-bubble tank that (1) consists of intersecting conical shells with web reinforcements at the intersections and (2) is subject to a uniform internal differential pressure is structurally efficient if all webs are planar.*

The Equivalence constrains the design of a tapered multi-bubble tank to a series of intersecting conical shells for which each intersection is a plane curve. This constraint is expressed in Eq. (18) which involves the total set of independent geometry descriptors $\Psi = \{\alpha, \beta, \gamma, r_1, r_2, v\}$ for each pair of adjoint bubbles with intersecting conical shells. The following four statements are equivalent if Eq. (18) is met:

1. the web's angle of deflection δ is constant.
2. the intersection curve is a plane curve.
3. the web is planar.
4. the tapered multi-bubble tank is structurally efficient.

Depending on the values for the set $\{\alpha, \beta, \gamma\}$, there are four cases:

Case 1. Cylindrical shells - Parallel axes of revolution
In this case, $\alpha = 0°$ and $\beta = \gamma = 0°$. The condition for structural efficiency (Eq. (18)) is always met, hence the angle δ is constant and the web is planar. Moreover, the angle δ is always equal to zero according to Eq. (7) because of the coefficients of the homogeneous equation $A = B = C = E = 0$. According to expectations, the multi-bubble tank is a cylindrical multi-bubble tank, i.e. the set $\{\Psi \mid \alpha = \beta = \gamma = 0°\}$, is inherently structurally efficient.

Case 2. Cylindrical shells - Intersecting axes of revolution
In this case, $\alpha = 0°$ and $\beta = \gamma \neq 0°$. The condition for structural efficiency (Eq. (18)) is met if $2\delta = \gamma$. Eq. (7) shows that the condition $2\delta = \gamma$ is met if $\gamma = 0°$ (i.e. Case 1) or if both cylinders have equal radii (i.e. $r_1 = r_2$). In other words, the tapered multi-bubble tank obtained as the intersection of two cylinders of equal radius whose axes are intersecting lines, i.e. the set $\{\Psi \mid \alpha = 0°, \beta = \gamma, r_1 = r_2\}$, is structurally efficient and the web is in an additional plane of symmetry.

Case 3. Conical shells - Parallel axes of revolution
In this case, $\alpha \neq 0°$ and $\beta \neq \gamma = 0°$. The condition for structural efficiency (Eq. (18)) is met if $\alpha = \beta$. Because of the coefficients of

Table 3
Numerical values of the geometry descriptors $\{\alpha, \beta, \gamma, r_1, r_2, v\}$ and numerical results of the angle δ, maximum value of the major principal stress σ_1 maximum across the shell and maximum value of the magnitude of displacement u for Cases 1 to 4.

Case	α [°]	β [°]	γ [°]	r_1 [m]	r_2 [m]	v [m]	δ [°]	$\sigma_{1,\,\max}$ [MPa]	$u_{\max}$ [mm]
1	0.0	0.0	0.0	2.254	2.126	2.266	0.0	134.66	9.51
2	0.0	6.0	6.0	2.254	2.254	2.266	3.0	133.57	7.48
3	1.5	1.5	0.0	2.254	2.126	2.266	0.08475	135.27	9.91
4	1.5	4.718	2.121	2.254	2.126	2.266	0.0	135.08	10.76

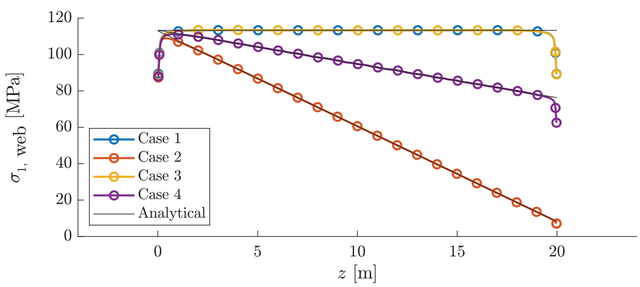

Fig. 10. Analytical (Eq. (19)) and FE stress results (Fig. 12) of the major principal stress averaged across the shell thickness in the web at the Y-junction.

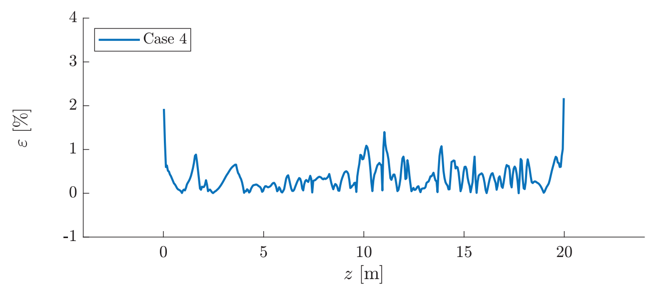

Fig. 11. FE stress results of the major principal stress in the web at the Y-junction for Case 4. This illustration shows the maximum stress across the shell thickness relative to the average stress across the shell thickness: $\varepsilon = \left|1 - \sigma_{\max}/\sigma_{\text{avg}}\right|$.

the homogeneous equation $A = B = C = 0$ if $\alpha = \beta$ and $\gamma = 0°$, Eq. (7) simplifies to

$$\tan\delta = \frac{E}{D} = \frac{r_1 - r_2}{v}\tan\alpha$$

and shows that δ is always nonzero unless $\alpha = \beta = 0°$ (i.e. Case 1) or if both cones have equal radii (i.e. $r_1 = r_2$). The tapered multi-bubble tank assembled as two conical shells of equal apex angle and whose axes are parallel lines, i.e. the set $\{\Psi \mid \alpha = \beta, \gamma = 0°\}$, is structurally efficient.

Case 4. Conical shells - Intersecting axes of revolution

In this case, $\alpha \neq 0°$ and $\beta \neq \gamma \neq 0°$. At least one solution for γ exists for every set of geometric descriptors $\{\alpha, \beta, r_1, r_2, v\}$ such that the condition for structural efficiency (Eq. (18)) holds. In contrast to Case 3 where the angles α and β have to be equal to each other due to the parallel axes of revolution ($\gamma = 0°$), this case shows the significance of the angle γ in the design degree of freedom of a structurally efficient tapered multi-bubble tank. The intersection of the axes of revolution at an angle γ in this case allows to design a structurally efficient tapered multi-bubble tank with unequal angles α and β. The inequality between α and β provides an additional taper degree of freedom for accommodating the tank in an arbitrary space.

5. Validation

This section is an objective validation of the analysis procedure from Sections 2–3 and the Equivalence that results. The finite element (FE) method is a generic and independent instrument for structural analysis. The commercial Siemens Simcenter 3D software is used in this analysis. The validation case is a tapered two-bubble tank closed with spherical two-bubble heads and without structural discontinuities for Cases 1 to 4 (Section 4). It is deliberately simple with few geometry descriptors (Table 3), but more complex geometries can be considered too. The angles α and β, the radii r_1 and r_2 and the separation distance v are randomly selected. The angles β and γ for Case 4 are calculated using Eqs. (7) and (18) such that the resulting angle δ is zero. A 3D tapered two-bubble structure with a length of 20 m is modelled by inserting the values of the geometry descriptors in the template from Fig. 4.

An FE model of the tapered two-bubble tank is created using CQUAD4 and CTRIA3 shell elements. Low internal differential pressure $p = 50$ kPa is applied. Shell thickness $t = 1$ mm is sufficient to sustain pressure safely using standard engineering materials. Mesh convergence analysis shows that an overall element size of 50 mm is sufficient, which leads to a total of 107 424 nodes for Case 4. The FE model of the tank is constrained with minimum statically determinate boundary conditions. Finally, Simcenter Nastran version 2212.0 is used to obtain the linear static solution for the 3D displacements u, major principal stress σ_1 and intermediate principal stress σ_2 with minor principal stress σ_3 equal to zero in plane stress conditions. All shell elements in the two-bubble tank are subject to a combination of membrane tensile load and bending. In standard FE procedure stress is calculated from the displacement field using equations from plate theory. Membrane stress is calculated from in-plane displacement degrees of freedom, whereas bending stress is calculated from out-of-plane displacement degrees of freedom and nodal rotations. Stress output is requested at the top and bottom surfaces of the shell element, because peak values occur at either shell surfaces.

Figs. 10 and 11 show the FE stress results of the major principal stress in the web at the Y-junction. They are the result of post-processing of the FE stress values in the two-bubble tanks shown in Fig. 12. Membrane stress is derived directly as the average value of stress at the top and bottom surfaces of the shell element and it is compared to the analytical stress values in Fig. 10. The analytical stress results of the major principal stress $\sigma_{1,\,\text{web}}$ in the web at the Y-junction is calculated from the division of Eq. (15) by the shell thickness t. Further reformulation of Eq. (15) using Eqs. (3) and (4) gives

$$\sigma_{1,\,\text{web}} = \frac{p}{t}\left(\frac{(v - x(z))\cos\gamma - z\sin\gamma}{\cos(\beta - \gamma)} + \frac{x(z)}{\cos\alpha}\right) \tag{19}$$

Eq. (19) is a linear function with respect to the longitudinal z-axis provided that the Equivalence holds and depends on the pressure p, shell thickness t and independent geometry descriptors $\{\alpha, \beta, \gamma, r_1, r_2, v\}$ with $x(z)$ the coordinates of the web (Eq. (5)). The analytical and FE stress results of $\sigma_{1,\,\text{web}}$ are approximately equal along the entire length of the tapered two-bubble tank for each case.

Displacements and the maximum stress across the shell thickness are used to identify bending stress. The maximum values of the major principal stress maximum across the shell thickness are added to Table 3 and are located at the connection of a sphere with a cylinder or cone. Fig. 11 shows that maximum stress across the shell thickness and average stress across the shell thickness are approximately equal at the Y-junction along the entire length of the tank. Displacements are limited to 0.5% of the largest radius in the entire model.

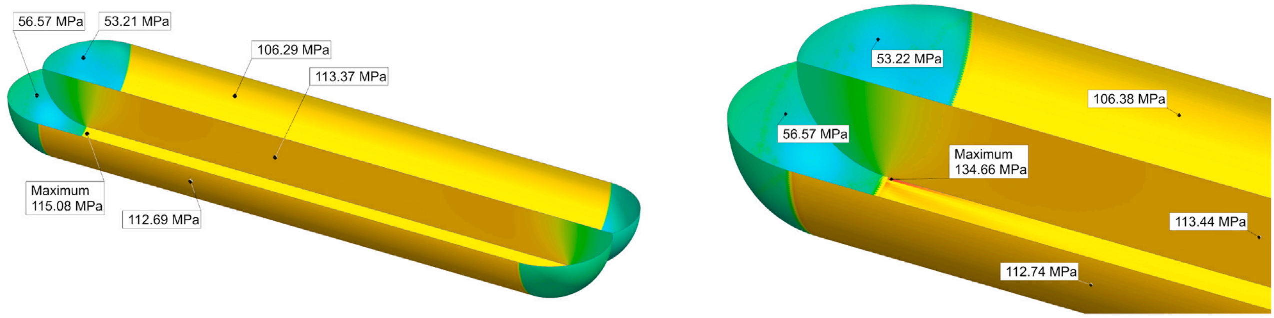

(a) Case 1. Cylindrical shells - Parallel axes of revolution

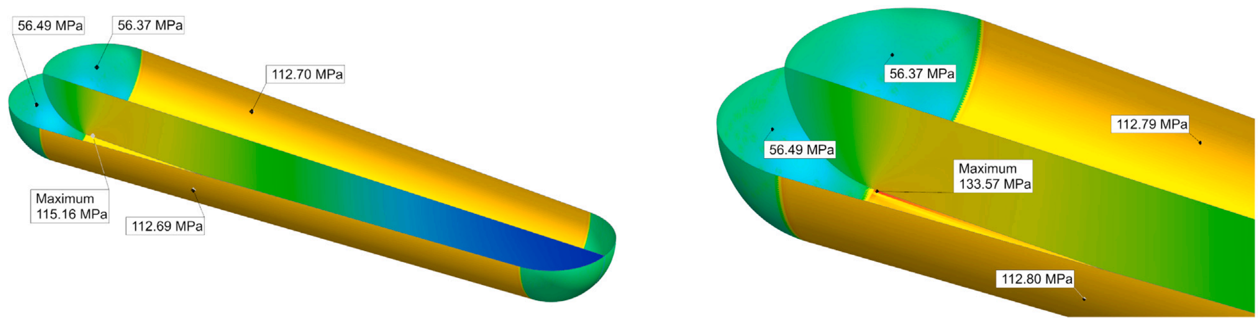

(b) Case 2. Cylindrical shells - Intersecting axes of revolution

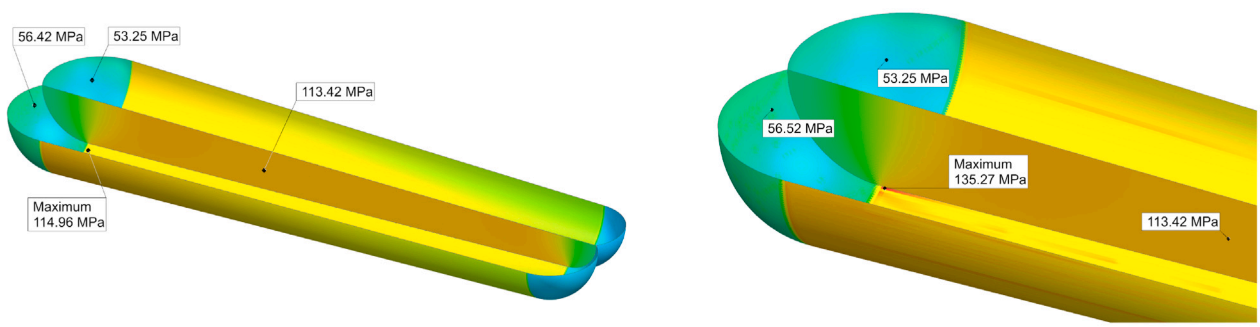

(c) Case 3. Conical shells - Parallel axes of revolution

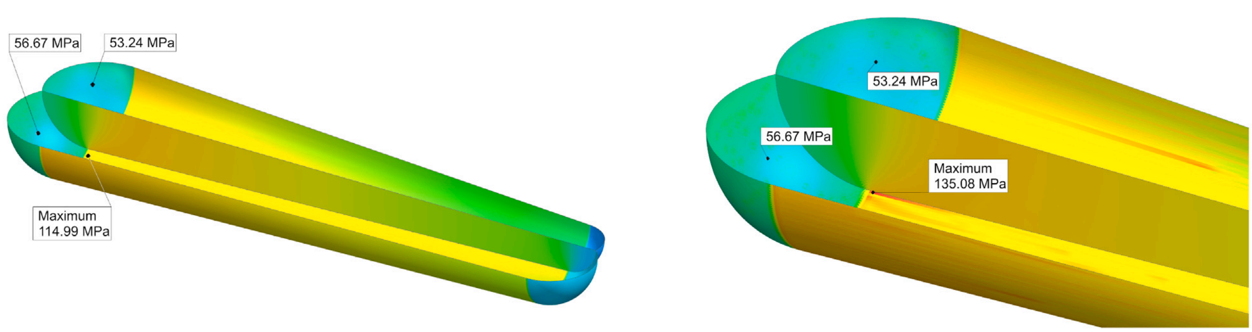

(d) Case 4. Conical shells - Intersecting axes of revolution

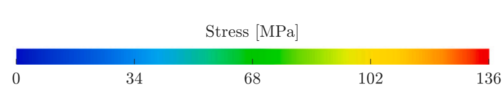

Fig. 12. Major principal stress in the tapered two-bubble tank subject to an internal pressure of 50 kPa with geometry descriptors listed in Table 3 for Cases 1 to 4. (left) Average value of stress at the top and bottom surfaces of the shell element and (right) maximum stress across the shell thickness. Only half of the two-bubble tank is shown because of symmetry and to visualize the stress components in the planar web at the inside of the tank.

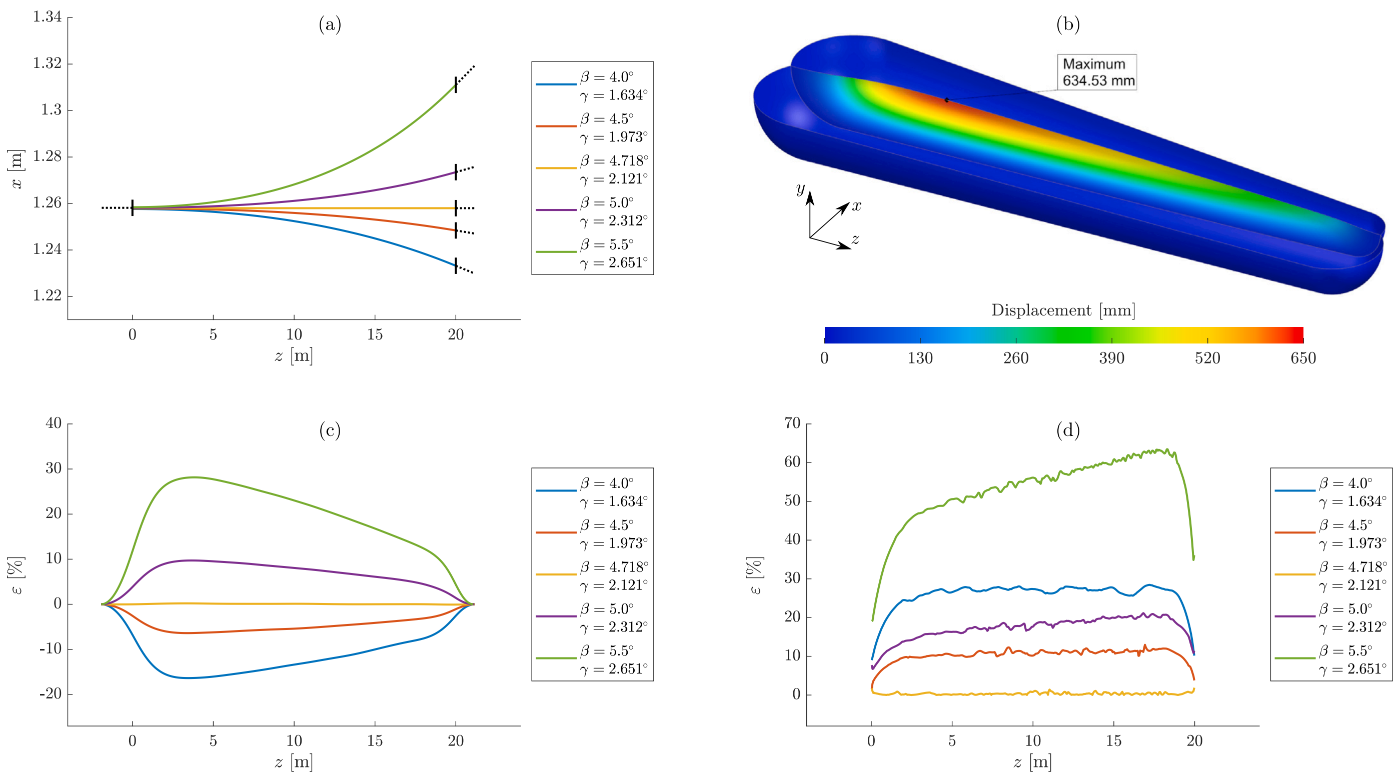

Fig. 13. FE displacement and stress results in tapered two-bubble tanks with different curvatures of the web and with fixed geometry descriptors $\{r_1, r_2, v\} = \{2.254, 2.126, 2.266\}$ m and $\{\alpha, \delta(0)\} = \{1.5, 0\}$ degrees. (a) Nonplanarity of the web for different values of β and γ (Eq. (5)). This illustration shows the web in the tapered structure (solid line) connected to the webs in the spherical structures (dotted lines). (b) Displacements along the x-axis in the tapered two-bubble tank with $\{\beta, \gamma\} = \{5.5, 2.651\}$ degrees. This illustration shows the absolute deformed model (1:1). (c) FE displacement results of the transverse displacements of the web in the plane of symmetry. This illustration shows the transverse displacements relative to the largest radius: $\varepsilon = u_x/r_1$ and Fig. 13(b) shows the absolute values of u_x for the model with $\beta = 5.5°$. (d) FE stress results of the major principal stress in the web at the Y-junction. This illustration shows the maximum stress across the shell thickness relative to the average stress across the shell thickness: $\varepsilon = \left|1 - \sigma_{\max}/\sigma_{\mathrm{avg}}\right|$.

FE results coincide with analytical results and the uniformity of the stress fields shows that the Equivalence holds and that the two-bubble tank is structurally efficient for each case. Fig. 12 also shows that stress components in the tank wall are constant along the length of the tank for cylindrical shells (Cases 1 and 2) and are linearly decreasing with approximately $p\tan(\alpha)/t$ and $p\tan(\beta-\gamma)/t$ for conical shells (Cases 3 and 4). Stress components in the web are (approximately) constant along the length of the tank for parallel axes of revolution (Cases 1 and 3) and are linearly decreasing with approximately $p\sin(\gamma)/t$ for axes of revolution intersecting at an angle γ (Cases 2 and 4).

6. Proof by contradiction

The FE results in Section 5 show the stress fields in thin-walled tapered two-bubble tanks that are in agreement with the Equivalence. Compliance with the Equivalence is a necessary condition for membrane stress to be dominant over bending stress. As a proof by contradiction, this section briefly shows that displacements and stresses increase if the condition from the Equivalence is violated so that the web is no longer a plane surface but a curved surface even if that deviation is only slight. Case 4 is repeated and the angles $\alpha = 1.5°$ and $\delta(0) = 0°$ are fixed for now, but geometry is slightly modified to violate the condition from the Equivalence. By increasing β from 4.0° to 5.5° in steps of 0.5° and calculating the corresponding angle γ for every value of β using Eq. (7), four different designs of a tapered two-bubble tank with a nonplanar web are created. Fig. 13(a) shows the resulting nonplanarity of the web in the plane of symmetry for each solution together with the structurally efficient solution $\{\beta, \gamma\} = \{4.718, 2.121\}$ degrees (Table 3). Edges of the tapered structure are at $z = 0$ m and $z = 20$ m. Parts of the web formed by the spherical two-bubble heads at both ends of the tank are added to show the structural continuity of the web.

Fig. 13(b) shows the absolute deformed tapered two-bubble tank subject to an internal pressure of 50 kPa for $\beta = 5.5°$ and a shell thickness of 1 mm. Maximum magnitude of the displacement vector occurs in the x-direction or transverse direction of the web in the plane of symmetry and is equal to 635 mm or 28.2% of the largest radius in the tank. Fig. 13(c) shows the transverse displacements of the web in the plane of symmetry for the models with other values of β and Fig. 13(d) shows the major principal stress in the web at the Y-junction. These two figures show for values of the angle β in the range from 4.0° to 5.5° that a tapered multi-bubble tank geometry exists in which displacements and stresses are minimum. This optimal geometry is the structurally efficient solution ($\beta = 4.718°$) and even small deviations from the ideally planar web result in large transverse displacements of the web and high stress peaks at the Y-junction. This result demonstrates the importance of a planar web to preserve structural efficiency and shows that the Equivalence should not be violated in the design of a tapered multi-bubble tank.

7. Conclusion

An analytical proof and an independent numerical validation show that the Equivalence is a fundamental rule in the design of a tapered multi-bubble tank under differential pressure. All web reinforcements have to be plane surfaces to guarantee a structurally efficient tapered conformable structure in which the orientation of the members align with the orientation of resulting forces which are transferred by each of the members. Based on this principle, tapered multi-bubble tanks are shown to have similar wall thickness and hoop stresses as for classical pressure tanks with an axi-symmetric layout such as cylindrical shells. This conclusion and construction guidelines provide the tank designer with a simple geometrical rule to assure from the start a structurally efficient tapered conformable low-pressure tank. However, with the high degree of sensitivity of stress peaks to geometry in general and web planarity in particular, both the designer and manufacturer should pay attention to precision.

CRediT authorship contribution statement

Joren Malfroy: Writing – original draft, Methodology, Conceptualization. **Ben Van Bavel:** Writing – review & editing. **Johan Steelant:** Writing – review & editing. **Dirk Vandepitte:** Writing – review & editing, Supervision.

Declaration of competing interest

The authors declare the following financial interests/personal relationships which may be considered as potential competing interests: Joren Malfroy reports financial support was provided by Research Foundation - Flanders (FWO).

Data availability

Data will be made available on request.

Acknowledgements

This work was supported by the Research Foundation - Flanders (FWO), Belgium, grant number 1SG1523N.

Appendix

Implicit equation of the first cone:

$$\begin{aligned}&G_{c,1}(x,y,z)\\&=x^2+y^2-(r_1-z\tan\alpha)^2\\&=x^2+y^2-r_1^2-z^2\tan^2\alpha+2r_1z\tan\alpha\end{aligned}$$

Implicit equation of the second cone:

$$\begin{aligned}&G_{c,2}(x,y,z)\\&=[(x-v)\cos\gamma+z\sin\gamma]^2+y^2\\&\quad-\left[r_2+((x-v)\sin\gamma-z\cos\gamma)\tan(\beta-\gamma)\right]^2\\&=(x-v)^2\cos^2\gamma+z^2\sin^2\gamma+2(x-v)z\cos\gamma\sin\gamma+y^2\\&\quad-r_2^2-2r_2(x-v)\sin\gamma\tan(\beta-\gamma)+2r_2z\cos\gamma\tan(\beta-\gamma)\\&\quad-(x-v)^2\sin^2\gamma\tan^2(\beta-\gamma)-z^2\cos^2\gamma\tan^2(\beta-\gamma)\\&\quad+2(x-v)z\sin\gamma\cos\gamma\tan^2(\beta-\gamma)\\&=(x-v)^2(\cos^2\gamma-\sin^2\gamma\tan^2(\beta-\gamma))+y^2\\&\quad+2(x-v)z\cos\gamma\sin\gamma(1+\tan^2(\beta-\gamma))\\&\quad+z^2(\sin^2\gamma-\cos^2\gamma\tan^2(\beta-\gamma))\\&\quad-r_2^2-2r_2(x-v)\sin\gamma\tan(\beta-\gamma)+2r_2z\cos\gamma\tan(\beta-\gamma)\end{aligned}$$

Implicit equation of the web:

$$\begin{aligned}G_w(x,z)&=G_{c,2}(x,y,z)-G_{c,1}(x,y,z)\\&=Ax^2+Bxz+Cz^2+Dx+Ez+F\end{aligned}$$

with

$$\begin{aligned}A&=-1+\cos^2\gamma-\sin^2\gamma\tan^2(\beta-\gamma)=-\frac{\sin^2\gamma}{\cos^2(\beta-\gamma)}\\B&=2\cos\gamma\sin\gamma(1+\tan^2(\beta-\gamma))=\frac{\sin2\gamma}{\cos^2(\beta-\gamma)}\\C&=\sin^2\gamma-\cos^2\gamma\tan^2(\beta-\gamma)+\tan^2\alpha\\&=-A-\tan^2(\beta-\gamma)+\tan^2\alpha\\D&=-2v(\cos^2\gamma-\sin^2\gamma\tan^2(\beta-\gamma))-2r_2\sin\gamma\tan(\beta-\gamma)\\&=-2v(1+A)-2r_2\sin\gamma\tan(\beta-\gamma)\\E&=-2v\cos\gamma\sin\gamma(1+\tan^2(\beta-\gamma))+2r_2\cos\gamma\tan(\beta-\gamma)-2r_1\tan\alpha\\&=-vB+2r_2\cos\gamma\tan(\beta-\gamma)-2r_1\tan\alpha\\F&=v^2(\cos^2\gamma-\sin^2\gamma\tan^2(\beta-\gamma))+2vr_2\sin\gamma\tan(\beta-\gamma)-r_2^2+r_1^2\\&=-vD-v^2(1+A)-r_2^2+r_1^2\end{aligned}$$

Simplification of Eq. (10):

$$\begin{aligned}&-A-\tan^2(\beta-\gamma)+\tan^2\alpha-B\tan\delta+A\tan^2\delta\\&=\frac{\sin^2\gamma}{\cos^2(\beta-\gamma)}+1-\frac{1}{\cos^2(\beta-\gamma)}-1+\frac{1}{\cos^2\alpha}\\&\quad-\frac{\sin2\gamma}{\cos^2(\beta-\gamma)}\tan\delta-\frac{\sin^2\gamma}{\cos^2(\beta-\gamma)}\tan^2\delta\\&=-\frac{1}{\cos^2(\beta-\gamma)}\left(\cos^2\gamma+\sin2\gamma\tan\delta+\sin^2\gamma\tan^2\delta\right)+\frac{1}{\cos^2\alpha}\\&=-\frac{1}{\cos^2(\beta-\gamma)}(\cos\gamma+\sin\gamma\tan\delta)^2+\frac{1}{\cos^2\alpha}\\&=-\frac{\cos^2(\gamma-\delta)}{\cos^2(\beta-\gamma)\cos^2\delta}+\frac{1}{\cos^2\alpha}\end{aligned}$$

References

[1] A. Zingoni, Stresses and deformations in egg-shaped sludge digestors: membrane effects, Eng. Struct. 23 (2001) 1365–1372.
[2] A. Zingoni, Stresses and deformations in egg-shaped sludge digestors: discontinuity effects, Eng. Struct. 23 (2001) 1373–1382.
[3] A. Zingoni, B. Mokhothu, N. Enoma, A theoretical formulation for the stress analysis of multi-segmented spherical shells for high-volume liquid containment, Eng. Struct. 87 (2015) 21–31.
[4] P. Jasion, K. Magnucki, A pressure vessel with a special barrelled shape, Ocean Eng. 263 (2022).
[5] M.D. Ardema, Structural weight analysis of hypersonic aircraft, NASA (1972).
[6] B. Van Bavel, Thermo-mechanical fatigue on a Y-junction of a cryogenic multi-lobe tank for hypersonic applications (Master's thesis), KU Leuven, Faculty of Engineering Science, Leuven, 2020.
[7] J. Malfroy, Design and optimization of a tapered multi-bubble tank for hypersonic aircraft (Master's thesis), KU Leuven, Faculty of Engineering Science, Leuven, 2022.
[8] J. Steelant, M. van Duijn, Structural analysis of the LAPCAT-MR2 waverider based vehicle, in: 17th AIAA International Space Planes and Hypersonic Systems and Technologies Conference, 2011.
[9] J. Steelant, T. Langener, The LAPCAT-MR2 hypersonic cruiser concept, in: 29th Congress of the International Council of the Aeronautical Sciences, (ICAS), 2014.
[10] J. Steelant, R. Varvill, C. Walton, S. Defoort, K. Hannemann, M. Marini, Achievements obtained for sustained hypersonic flight within the LAPCAT-II project, in: 20th AIAA International Space Planes and Hypersonic Systems and Technologies Conference, 2015.
[11] M. Rodríguez-Segade, S. Hernández, J. Díaz, D. López, A. Baldomir, STRATOFLY project approaches for innovative structural schemes and modelization of hypersonic aircraft and space vehicles, in: International Conference on Flight Vehicles, Aerothermodynamics and Re-Entry Missions & Engineering (FAR), 2019.
[12] M. Rodríguez-Segade, S. Hernández, J. Díaz, A. Baldomir, D. López, Global and local models for the structural analysis of the hypersonic STRATOFLY vehicle, in: 23rd AIAA International Space Planes and Hypersonic Systems and Technologies Conference, 2020.
[13] M. Rodríguez-Segade, S. Hernández, J. Díaz, Multi-bubble scheme and structural analysis of a hypersonic stratospheric flight vehicle, Aerosp. Sci. Technol. 124 (2022).
[14] Final report of the X-33 liquid hydrogen tank test investigation, in: NASA Marshall Space Flight Center, Huntsville, 2000.
[15] V. Mukhopadhyay, Structural concepts study of non-circular fuselage configurations, in: SAE/AIAA World Aviation Congress, (WAC-67) 1996.
[16] V. Mukhopadhyay, J. Sobieszczanski-Sobieski, I. Kosaka, G. Quinn, G. Vanderplaats, Analysis, design, and optimization of non-cylindrical fuselage for blended-wing-body vehicle, J. Aircr. 41 (2004) 925–930.
[17] M. Bishara, P. Horst, H. Madhusoodanan, M. Brod, B. Daum, R. Rolfes, A structural design concept for a multi-shell blended wing body with laminar flow control, Energies 11 (2018) 383.
[18] S.H. Cho, C. Bil, J. Bayandor, BWB military cargo transport fuselage design and analysis, in: 26th Congress of the International Council of the Aeronautical Sciences, (ICAS), 2008.

[19] N. Viola, et al., Main challenges and goals of the H2020 STRATOFLY project, Aerotecnica Missili Spazio (2021).

[20] F. Geuskens, S. Koussios, O. Bergsma, A. Beukers, Non-cylindrical pressure fuselages for future aircraft, in: 49th AIAA/ASME/ASCE/AHS/ASC Structures, Structural Dynamics, and Materials Conference, 2008.

[21] F. Geuskens, O. Bergsma, S. Koussios, A. Beukers, Analysis of conformable pressure vessels: Introducing the multi-bubble, AIAA J. 49 (2011) 1683–1692.

[22] F. Geuskens, J. Tielking, S. Koussios, A. Beukers, Modified linear-membrane formulation for the pressurized torus and multitorus, AIAA J. 51 (2013) 2114–2125.

[23] K. Sowiński, K. Magnucki, Shaping of dished heads of the cylindrical pressure vessel for diminishing of the edge effect, Thin-Walled Struct. 131 (2018) 746–754.

[24] W. Flügge, Stresses in shells, 2nd Ed., Springer-Verlag, Berlin, 1973.